

# Structure Effects on Coulomb Dissociation of ${}^8\text{B}$

F.M. Nunes<sup>1)</sup>, R. Shyam<sup>2)</sup> and I.J. Thompson<sup>3)</sup>

<sup>1)</sup> Department of Physics, Instituto Superior Tecnico, Lisbon, Portugal

<sup>2)</sup> Saha Institute for Nuclear Physics, Calcutta, India

<sup>3)</sup> Department of Physics, University of Surrey, Guildford, UK

**Abstract.** Coulomb Dissociation provides an alternative method for determining the radiative capture cross sections at astrophysically relevant low relative energies. For the breakup of  ${}^8\text{B}$  on  ${}^{58}\text{Ni}$ , we calculate the total Coulomb Dissociation cross section and the angular distribution for E1, E2 and M1. Our calculations are performed first within the standard first order semiclassical theory of Coulomb Excitation, including the correct three body kinematics, and later including the projectile-target nuclear interactions.

We study the dependence of the Coulomb Dissociation cross section on the structure models assumed for the projectile. A range of potential models for  ${}^7\text{Be}+p$  are compared: we look at the effect of potential shapes, deformation and inclusion of inelastic channels in the projectile states. We analyse the relative E1 and E2 components and investigate the relation between the measured cross section and the S-factor  $S_{17}$ . Preliminary Coulomb-nuclear interference results are presented.

## 1. Introduction

Coulomb Dissociation (CD) experiments have brought new insight to the low energy capture reaction cross section  ${}^7\text{Be}(p,\gamma){}^8\text{B}$  which is a crucial ingredient for the solar neutrino puzzle [1]. The main idea resides on the fact that in suitable conditions, solely the Coulomb field is responsible for the breakup of the projectile, and nuclear uncertainties in the projectile-target interaction do not affect the total cross section. On the other hand, all CD measurement are *contaminated* by a non-negligible E2 component and although the astrophysical S-factor  $S_{17}$  (related to the  ${}^7\text{Be}$  proton capture rate at  $E = 20$  KeV) is determined by the E1 component only, to extract information from the CD data requires information on the E2 contribution. In this work we study the dependence of the total CD cross section on the structure models assumed for the projectile.

The experimental state of the art is very encouraging. The first Coulomb Dissociation measurements were performed at RIKEN [2] using a heavy target, a  ${}^8\text{B}$  beam of 46.5 MeV/A and complete kinematics. There have also been some measurements on a lighter target at Notre Dame [3] with a  ${}^8\text{B}$  beam of 3.225 MeV/A where only one of the fragments was detected. Recently the experiment at RIKEN was repeated with better statistics and a wider angular range in order to obtain more

information on the E2 contribution. Coulomb Dissociation of  $^8\text{B}$  being measured at relativistic energies in GSI [5] will soon be available.

Considerable theoretical effort has been offered to clarifying the relation between the Coulomb Dissociation process and the direct capture reaction. It is generally believed that as long as the minimum impact parameter is larger than the sum of the two nuclei radii plus a few fm, the nuclear effects as well as nuclear-Coulomb interference can be neglected. This appears to be the case [6] for the RIKEN experiment. Higher order terms have been discussed, namely it has been suggested that E1-E2 interference can partially cancel the E2 contribution [7]. For the purpose of this work, we will consider only E1, E2 and M1 contributions to first order, and including proper three body kinematics[8], and then explore in a preliminary way the true effects of nuclear excitations.

## 2. Virtual Photon Number

Assuming that the nuclear interaction of projectile-target is weak and that post-acceleration effects are small, the Coulomb Dissociation process can be treated semi-classically [9] in which the projectile-target relative motion takes place on a Rutherford trajectory. In first order, the differential cross section is the sum of the electromagnetic multipole components and can be written as a product of a virtual photon number VPN (depending only on the kinematics of the projectile-target relative motion and the excitation energy), and a photo-disintegration cross section of the projectile (defining the internal structure of the projectile):

$$\frac{d\sigma_{E\lambda}^{CD}}{d\Omega dE_\gamma} = \frac{1}{E_\gamma} \frac{dn_{E\lambda}}{d\Omega} \sigma_{E\lambda}^{photo} \quad (1)$$

The differential virtual photon number (as a function of the relative energy of the projectile fragments and the scattering angle) determines which parts of the energy spectrum of the projectile are relevant for a particular set-up of a Coulomb

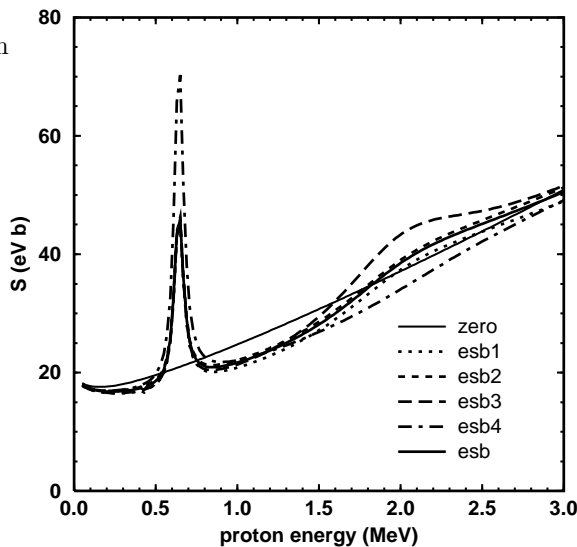


Figure 1: The effect on the proton capture S-factor of variations in the nuclear interaction for the continuum  $^8\text{B}$  states.

dissociation process. The lower part of the projectile spectrum is enhanced for the lower beam energies and the smaller scattering angles. In the low-energy experiment of [3], where  $E_{beam} = 3.225$  MeV/A and  $\theta \simeq 45^\circ$ , the E1 VPN is a slowly decreasing function of  $E_{rel}$ , so we expect the CD cross section will be sensitive to variations in the negative parity continuum of  ${}^8\text{B}$ . On the other hand, the E2 VPN decreases steeply thus the CD cross section will be mainly sensitive to the lower energy part of the positive parity continuum of  ${}^8\text{B}$ .

### 3. Structure Models for ${}^8\text{B}$

The breakup of  ${}^8\text{B}$  proceeds through E1 into  $1^-, 2^-, 3^-$  and through E2 (and M1) into  $0^+, 1^+, 2^+, 3^+$ . The ground state (g.s.) of  ${}^8\text{B}$  ( $2^+$ ) can be qualitatively described as  $p+{}^7\text{Be}$  in a  $p_{3/2}$  relative motion. There are no resonances in the continuum for the negative parity states up to 3 MeV, which leaves some freedom for the parameter choices in potential models [11]. There are two low lying resonances: a  $1^+$  state at  $E = 0.63$  MeV that is quite narrow, and a broader  $3^+$  state at  $E = 2.18$  MeV. The constraint imposed by these two resonances accepts a wide range of potential models.

#### 3.1. Uncertainties in the continuum of ${}^8\text{B}$

First we evaluate the uncertainty associated with the nuclear interaction in the continuum, which is mainly related to the negative parity states. For this we take the model from [7] [esb] and modify by  $\simeq 20\%$  the strength of the nuclear interaction for all but the  $2^+, 1^+, 3^+$  states [esb1, esb2, esb3, esb4]. In fig. 1 we show the resulting S-factor as a function of the proton CM energy. In fig. 2 we show the differential cross section for the Coulomb dissociation on a  ${}^{58}\text{Ni}$  target for  $E_{beam} = 3.225$  MeV/A (the Notre Dame experimental conditions [3]). The Coulomb dissociation calculations use the method of [9] with proper three-body kinematics [8]. In these figures we also include the results for the extreme case where no nuclear interaction is included in the  ${}^7\text{Be}$ -p continuum [zero].

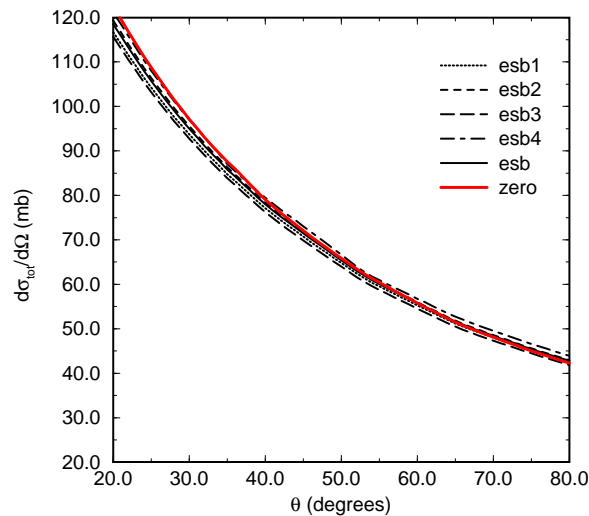


Figure 2: Effects of continuum nuclear potentials on the CD cross section at 3.225 MeV/A.

The very low energy S-factor is not affected by these small variations on parameters for the continuum interactions (for the set of models under consideration  $S(E=50 \text{ keV})$  differ by less than 1%) however there are considerable differences in the S-factor curves above 0.4 MeV. We find that the breakup cross section at low energies is not strongly influenced by these parameter variations. Thus the uncertainties in the nuclear interactions for the  ${}^8\text{B}$  scattering states have a negligible influence on the Coulomb Dissociation differential cross section for the Notre Dame set-up. This conclusion holds for lower and higher beam energies.

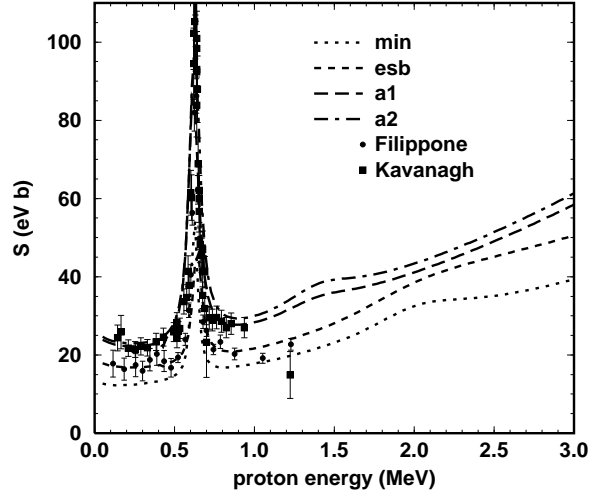


Figure 3: The proton capture S-factor for a set of structure models for  ${}^8\text{B}$  (data from [17, 18] with the updated normalisations).

### 3.2. Shape parameters - Overall normalisation

In this section we compare the results obtained with different potential models. All potential models reproduce the binding energy and the energy of the two resonances. We choose four models from the literature based on a Woods-Saxon shape: [esb] [7] with  $R = 2.39 \text{ fm}$  and  $a = 0.52 \text{ fm}$ ; [kim] [11] with  $R = 0.52 \text{ fm}$  and  $a = 0.52 \text{ fm}$ ; [a1] and [a2] with the same shape parameters as [kim] but including deformation of the  ${}^7\text{Be}$  nuclear and reorientation effects [12]; [c1] and [c2] that consist on the extension of [a1] and [a2] including the inelastic channels corresponding to all excited states of the  ${}^7\text{Be}$  core

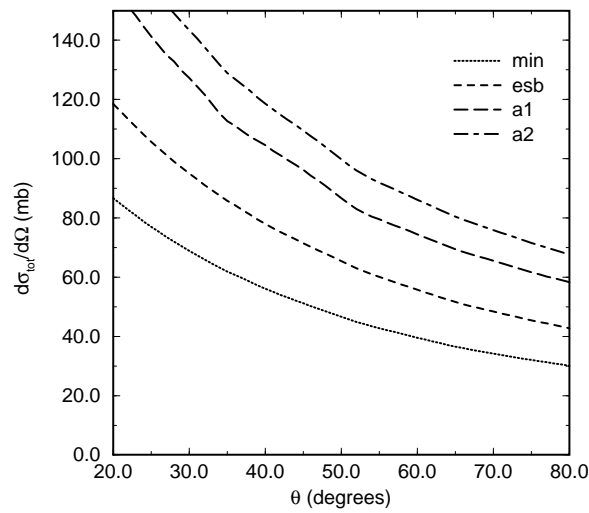


Figure 4: The dependence of the differential Coulomb dissociation cross section for a set of structure models for  ${}^8\text{B}$ .

[12]. We also include the predictions for what we call the minimum model [**min**] where we take low values for both radius and diffuseness parameters verging on the unrealistic ( $R = 2.0$  fm and  $a = 0.4$  fm).

The calculated S-factors for this set of models are presented in fig. 3. It is now well accepted that all potential models predict roughly the same low energy behaviour for the S-factor apart from an overall normalisation [10, 12]. This same effect is seen in the differential cross section for Coulomb dissociation and is clearly shown in fig. 4 where we plot the results for  ${}^8\text{B}$  Coulomb dissociation on a  ${}^{58}\text{Ni}$  target for  $E_{beam} = 3.225$  MeV/A for some of the models. We find that the CD cross section is not very sensitive to the differences in the  ${}^8\text{B}$  spectrum above  $E_{rel} \sim 0.5$  MeV. In fig. 5 we show the ratio between E1 and E2 contributions to the differential cross section for some of the models. We find that the curves differ by a constant factor, and that the models that have a larger E1 fraction predict a smaller total cross section.

At Notre Dame it was not possible to measure the differential cross section. Instead the data refers to a total cross section integrated from  $\theta = 39^\circ - 51^\circ$ . In table 1 the results obtained for the total cross section predicted for the Notre Dame experiment are shown. As in [8], the predictions are much larger than the data. We confirm this result, and that it is not possible to reproduce the measured result for any of our models of  ${}^8\text{B}$  structure. One could at first think that the E2 contribution was being over estimated, but in some cases even just the E1 cross section is too large (see table 1).

This great mismatch with the low-energy data may signify that the  ${}^7\text{Be}$  component of the  ${}^8\text{B}$  states is very small and that other cluster components are more important. This is unlikely since the models are able to reproduce the capture data within a reasonable accuracy. If

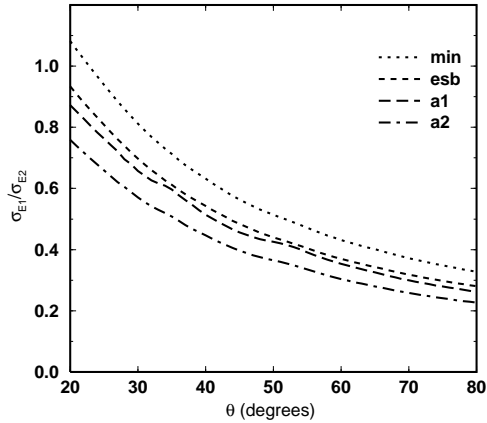


Figure 5: The E1 to E2 ratio in the Coulomb dissociation for a set of structure models of  ${}^8\text{B}$  incident at 3.225 MeV/A on  ${}^{58}\text{Ni}$ .

larger E1 fraction predict a smaller total cross section.

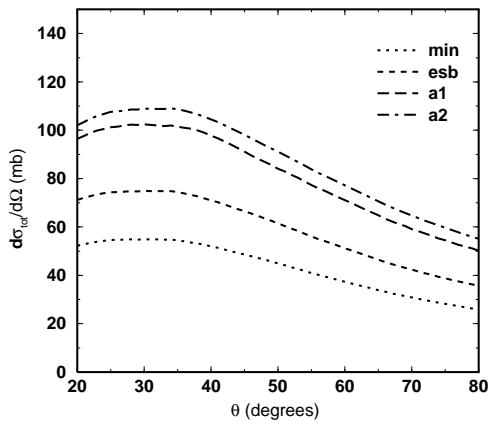


Figure 6: The dependence of the Coulomb dissociation cross section on  ${}^{197}\text{Au}$  on the structure model for  ${}^8\text{B}$ .

Model	$\frac{\sigma(tot)}{\sigma(ruth)}$	$\frac{\sigma(E1)}{\sigma(ruth)}$	$\frac{\sigma(E2)}{\sigma(E1)}$	S(50 keV) (eV b)
min	$2.07 \times 10^{-2}$	$0.75 \times 10^{-2}$	1.74	12.7
esb	$2.89 \times 10^{-2}$	$0.95 \times 10^{-2}$	2.04	17.9
kim	$3.88 \times 10^{-2}$	$1.16 \times 10^{-2}$	2.35	22.5
a1	$3.86 \times 10^{-2}$	$1.23 \times 10^{-2}$	2.14	23.9
a2	$4.41 \times 10^{-2}$	$1.27 \times 10^{-2}$	2.48	24.7
c1	$3.39 \times 10^{-2}$	$1.06 \times 10^{-2}$	2.20	20.9
c2	$4.04 \times 10^{-2}$	$1.17 \times 10^{-2}$	2.46	22.8
exp	$(0.68 - 1.09) \times 10^{-2}$			

Table 1: The results obtained for the total Coulomb Dissociation cross section of  ${}^8\text{B}$  on  ${}^{58}\text{Ni}$ , for a set of  ${}^8\text{B}$  models.

that were the case then one would be in disagreement with microscopic predictions [13]. The mismatch with the data can alternatively mean that there is something missing in the reaction theory used to describe the process: higher order contributions inducing E1-E2 or Coulomb-nuclear interference may play a more relevant role than what was initially thought.

From our predictions it is clear that even if the models were in agreement with the experimental result it would still be hard to distinguish between models since some models predict similar cross sections but have different E1 and E2 components and thus predict quite different low energy S-factor for the capture process (dominated by E1 only). From this data there is no indication as to the relative amount of E1 and E2. Thus it may be helpful to perform measurement at different beam energies, different angular ranges, or using different targets in order to get more information on the relative amounts of E1 and E2 contributions.

We also show (fig. 6) the resulting differential cross section if the  ${}^{58}\text{Ni}$  target were replaced by a  ${}^{197}\text{Au}$  target. This is one of the experiments that will be run in a few months [14].

#### 4. Improving the reaction theory

Given the difficulties that arose in trying to understand the existing Notre Dame data we decided to improve the reaction theory by taking nuclear-excitation effects into account. We performed prior-DWBA breakup calculations by discretising the continuum, including  $s_{1/2}$ ,  $p_{1/2}$ ,  $p_{3/2}$ ,  $d_{3/2}$ ,  $d_{5/2}$  partial waves up to  $E(\text{p-}{}^7\text{Be})=3$  MeV. The results shown in fig. 7 use 13 bins (9 bins of 100 keV centred at 0.15; 0.25; ...; 0.95 MeV and 4 bins of 500 keV centred at 1.25; 1.75; 2.25; 2.75), and in fig. 8 use 6 bins (4 bins of 250 keV centred at 0.125; 0.375; 0.625; 0.875 MeV and 2 bins of 1000 keV centred at 1.5; 2.5) and use  $l_{max} = 600\hbar$  and  $R_{max} = 300$  fm for the T-matrix integrals.

The E1 and E2 multipoles give cross sections (long-dashes in fig. 7) which reproduce the previous semiclassical results at forward angles. They agree at all angles (short-dashes in fig. 7) if the  $r^{-\lambda-1}$  multipoles are extrapolated to small radii. This point-projectile approximation (made in the semiclassical method) becomes invalid for scattering angles larger than  $20^\circ$ . However, at larger angles and smaller impact parameters, when the g.s. wavefunction of the projectile overlaps with the target interior, nuclear effects become simultaneously important.

Using a Becchetti-Greenlees [16] proton potential, and a  ${}^7\text{Li}$  potential [15] for  ${}^7\text{Be}$ , the pure nuclear breakup (dot-dashed in fig. 7) becomes significant beyond  $25^\circ$ . When nuclear and Coulomb multipoles are included coherently, there are already small effects below  $20^\circ$ , a large Coulomb-nuclear interference minimum between  $25^\circ$  and  $50^\circ$ , and a nuclear-dominated peak at  $75^\circ$  (solid-line in fig. 7). This large nuclear effect is present even though the elastic Coulomb + nuclear cross section only drops to 90% of the Rutherford cross section at  $70^\circ$ , because of the large halo-like size of proton wavefunction in the g.s. of  ${}^8\text{B}$ .

Fig. 8 shows the effects of the  ${}^8\text{B}$  structure on the pure-Coulomb and on the DWBA nuclear+Coulomb predictions. The dependencies on structure are largely similar in both cases, although the differences between the deformed-core models (a1 and a2) is reduced in the DWBA predictions. In all  ${}^8\text{B}$  models the interference

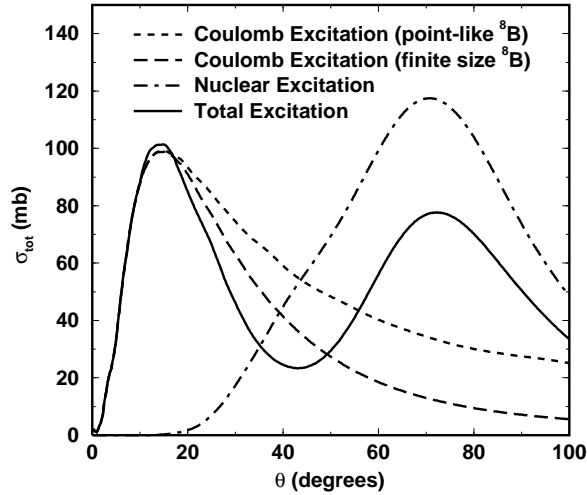


Figure 7: The quantum mechanical calculations for the differential Coulomb dissociation cross section using [esb].

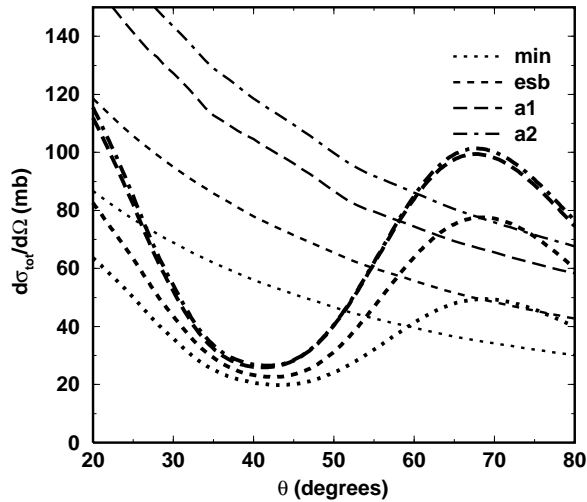


Figure 8: The  ${}^8\text{B}$  model dependence of the differential cross section within a 1 step quantum calculation (thick lines) compared with the semi-classical calculations.

minimum between  $30^\circ$  and  $50^\circ$  is present, and we begin to understand the low cross sections measured between  $31^\circ$  and  $59^\circ$  in the ND experiment. The horizontal-axis on both figures 7 and 8 refers to the scattering angle  $\theta(^8\text{B}^*)$ .

### Acknowledgments

UK support from the EPSRC grants GR/J/95867 and Portuguese support from JNICT PRAXIS/PCEX/P/FIS/4/96 are acknowledged

### References

- [1] J.N. Bahcall, *Neutrino Astrophysics* (Cambridge University Press, New York, 1989)
- [2] T. Motobayashi et al., Phys. Rev. Letts. **73** (1994) 2680
- [3] Johannes von Schwarzenberg et al., Phys. Rev. **C53** (1996) R2598
- [4] T. Kikuchi et al., Phys. Letts. **B391** (1997) 261
- [5] Klaus Suemmerer, *private communication*, December 1997
- [6] R. Shyam, I.J. Thompson and A.K. Dutt-Mazumder, Phys. Letts. **B371** (1996) 1
- [7] H. Esbensen and G. Bertsch, Nucl. Phys. **A600** (1996) 37
- [8] R. Shyam and I.J. Thompson, Phys. Letts. **B415** (1997) 315
- [9] K. Alder and A. Winther, *Electromagnetic Excitation*, (North Holland, Amsterdam, 1975)
- [10] F.C. Barker, Aust. J. Phys. **33** (1980) 177
- [11] K.H. Kim, M.H. Park and B.T. Kim, Phys. Rev. **C53** (1987) 363
- [12] F. Nunes, R. Crespo and I.J. Thompson, Nucl. Phys. **A615** (1997) 69, erratum **A627** (1997) 747, nucl-th/9709070
- [13] B.A. Brown, A. Csóto and R. Sherr, Nucl. Phys. **A597** (1996) 66
- [14] J.J. Kolata, *private communication*, December 1997
- [15] Z. Moroz et al., Nucl. Phys. **A 381** (1982) 294
- [16] F.D. Becchetti and G.W. Greenlees, Phys. Rev. **182** (1969) 1190
- [17] B.W. Filippone et al., Phys. Rev. Letts. **50** (1983) 412
- [18] W. Kavanagh et al., Bull. Amer. Soc. **14** (1969) 1209